# Determination of dissociative fragment-adsorbate interaction energy during chemisorption of the diatomic molecule HCl on Si(100)

Ming-Feng Hsieh (謝明峰), Jen-Yin Cheng (鄭人齊), Jenq-Cheng Yang (楊正成), and Deng-Sung Lin (林登松)*
*Department of Physics, National Tsing Hua University, 101 Kuang-Fu Road, Section 2, Hsinchu 30013, Taiwan, Republic of China and Institute of Physics, National Chiao Tung University, 1001 Ta-Hsueh Road, Hsinchu 30010, Taiwan, Republic of China*

Karina Morgenstern
*Institut für Festkörperphysik, Leibniz Universität Hannover, Appelstraße 2, D-30167 Hannover, Germany*

Woei-Wu Pai (白偉武)
*Center for Condensed Matter Sciences, National Taiwan University, Taipei 106, Taiwan, Republic of China*
(Received 17 September 2009; published 29 January 2010)

This study investigates the surface chemistry and the ordering characteristics of coadsorbed hydrogen and chlorine atoms, generated by the exposure of the Si(100) surface to gas-phase HCl molecules at various substrate temperatures, by scanning tunneling microscopy (STM), core-level photoemission spectroscopy, and Monte Carlo simulation. Experimental results show that saturation exposure to HCl causes all surface dangling bonds to be terminated by the two fragments H and Cl atoms and that the number of H-terminated sites exceeds that of Cl-terminated ones by more than 10%. This finding suggests that, in addition to the dominant dissociative chemisorption, atomically selective chemisorption or atom abstraction occurs. STM images reveal that some Cl-terminated sites form patches with a local $2 \times 2$ structure at 110 K and that the degree of ordering is reduced as the substrate temperature increases. Results of Monte Carlo simulations demonstrate the importance of including dissociative fragment-adsorbate interactions during the random adsorption of diatomic molecules. Comparing the correlations between Cl-terminated sites identified from STM images and those predicted by simulation reveals two effective interaction energies of $8.5 \pm 2.0$ and $3.5 \pm 2.0$ meV between a dissociative fragment Cl atom and a nearest neighboring Cl adsorbates in the same dimer row and in the adjacent row, respectively.

DOI: 10.1103/PhysRevB.81.045324 PACS number(s): 68.43.Hn, 68.43.Mn, 68.37.Ef, 68.47.Fg

## I. INTRODUCTION

A molecule or atom in close proximity to a solid surface interacts with the substrate; the interaction between the molecule or atom and the substrate, termed as adsorbate-substrate interaction (ASI), determines the type of reactions that occurs. Once adhered to the surface, the molecule or atom becomes an adsorbate and adsorbate-adsorbate interactions (AAIs) can occur directly by electrostatic repulsion owing to their charges[1] or indirectly mediated by substrate reconstruction,[2] lattice strain,[3] or surface states.[4,5] ASIs and AAIs are of great importance in a large variety of fundamental and technical areas in surface science, thin film growth, heterogeneous catalysis, and chemical sensing.[6] AAIs are typically weaker than ASIs but can lead to reconstructions or pattern formations on surfaces.[3,7,8] AAIs also change the sticking probabilities of molecules and the diffusivities of adsorbates.[9,10]

Often omitted in discussions of a surface process is that the single term "adsorbate" in AAIs and ASIs can refer to several species and to several bonding conditions and that AAIs and ASIs may vary from place to place on a surface, depending on the local adsorbate distributions. For example, multiatomic molecules may dissociate into their constituent fragments when they impinge on a surface.[11] In a simple case, the two separated fragments of a diatomic gas molecule, *AB*, react with a surface and form two new bonds, Su-*A* and Su-*B* (where Su denotes the surface), in a reaction that is called dissociative chemisorption,

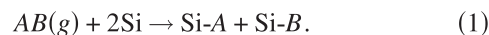

$$AB(g) + 2\text{Si} \rightarrow \text{Si-}A + \text{Si-}B. \quad (1)$$

Else, a surface abstracts atom *A* from an incident *AB* molecule to form a single bond Su-*A* and the *B* is ejected back to the gas phase; this reaction is called *A*-selective abstraction (or simply *A* abstraction),[12–14]

$$AB(g) + \text{Si} \rightarrow \text{Si-}A + B(g). \quad (2)$$

The individual probability of the above-mentioned two channels and unreactive scattering varies with many parameters such as the translational energy of the gas molecules, substrate temperature, and adsorbate coverages.[15–17] For example, the reaction probability of single F abstraction of $F_2$ on Si(100) increases from ~0.1 at zero F coverage ($\theta_F$) to a peak value of ~0.3 at $\theta_F \cong 0.5$ ML and then falls to 0 at saturation coverage.

Before Su-*A* or Su-*B* bonds are formed, in either of the two chemisorption mechanisms, fragment *A* or *B* can readily interact not only with the substrate but also with other fragments or adsorbates, which are previously adsorbed fragments. When a chemisorption process is completed, the fragment-fragment or fragment-adsorbate interactions develop into AAIs. Strong effective repulsive forces have been found to exist between two dissociated fragments by observing the well-separated pairwise adsorption of diatomic molecules and by examining the empirical "eight-site rule" that excludes the adsorption of the second atom of a dissociated molecule at the eight neighboring sites.[11] Since the fragment-

 ©2010 The American Physical Society

fragment or fragment-adsorbate interactions are transient and many-body effects, quantitative information of these two interactions is difficult to obtain.

The chemisorption and interaction of chlorine- and hydrogen-containing molecules on group-IV semiconductor surfaces are of great technological importance in the semiconductor industry.[18] Among the semiconductor gases, HCl gas is a prototypical heteronuclear diatomic molecule and has been commonly applied in reduced-pressure chemical vapor deposition to grow silicon, germanium, and GeSi alloys.[19] HCl chemistry is also important in the etching of silicon.[20] Both theoretical and experimental studies of the adsorption of HCl on Ge(100) and Si(100) surfaces have been performed.[21–24] HCl molecules are suggested to dissociate upon collision with the Si(100) surface. Each of the two dissociation fragments subsequently terminates one surface dangling bond (DB).

This investigation examines the temperature-dependent ordering characteristics of mixed adsorbates resulting from chemisorption of a diatomic gas. The energies of interaction between adsorbates and a dissociated fragment are determined experimentally. Specifically, both synchrotron-radiation core-level photoemission spectroscopy and scanning tunneling microscopy (STM) are used to observe mixed H- and Cl-terminated Si(100) surfaces that are saturated by gaseous HCl. In this work, both the spectroscopic and microscopic techniques (photoemission and STM) show that the number of H-termination sites exceeds that of Cl-terminated ones. Cl-terminated sites are found to form local $2\times2$ structure and zigzag chains. The degree of Cl-adsorbate ordering increases as the substrate temperature decreases, suggesting a kinetic ordering of adsorption of fragment Cl atoms. Introducing repulsive interaction energies between the fragment Cl atoms and the nearest neighboring Cl adsorbates in the Monte Carlo simulation yields populations and distributions of the adsorbed Cl and H atoms that resemble closely those obtained from STM images.

## II. EXPERIMENTAL DETAIL

A core-level photoemission experiment was performed at the Synchrotron Radiation Research Center in Taiwan. It involved a $\mu$-metal-shielded ultrahigh vacuum (UHV) chamber with a base pressure of $1\times10^{-10}$ torr. Light from the 1.5 GeV storage ring was dispersed by a spherical grating monochromator. The photocurrent from a gold mesh positioned in the synchrotron beam path was monitored to measure the relative incident photon beam flux. Photoelectrons were collected at 45° from the surface normal and analyzed using a 125 mm hemispherical analyzer. The overall energy resolution was better than 120 meV. In decompositions of core-level spectra, all fittings were least-squares fittings and each component that consisted of a pair of spin-orbit split doublets was assumed to have the same Voigt line shape. The STM experiments were conducted in another UHV chamber. All images were recorded in constant current mode at room temperature. Low tunneling currents (240 pA or less) were used; no diffusion or desorption of H sites and Cl sites was observed on the HCl-saturated Si(100) surface.

The Si(100) samples were sliced from doped antimony with a resistance of about 0.01 Ω cm. In both chambers, they were outgassed at ~800 K over 16 h under UHV conditions. Clean Si(100) surfaces were prepared by direct Joule heating at ~1400 K. The substrate was heated by passing a controlled dc directly through the sample. In the adsorption experiment at low temperature, the substrate was cooled to 110 K using liquid $N_2$. The substrate temperature $T_s$ was measured postfacto using a type-K thermocouple that was attached by epoxy to the front of the sample; the results were reproducible to within 15 K. The Si(100)-$2\times1$:H monohydride surface was prepared by 600 K saturation exposure of the clean Si(100) surface to atomic H. Atomic hydrogen was produced by backfilling the chamber in the presence of a hot tungsten filament at ~5 cm away from the sample. The Si(100)-$2\times1$:Cl monochloride surface was prepared by 300 K saturation exposure of the clean Si(100) surface to $Cl_2$. Ultrapure $Cl_2$ and HCl gases were introduced into the chamber through precision leak valves and stainless steel tubes that face the samples. During $Cl_2$ and HCl exposure, the chamber background pressure was about $5\times10^{-9}$ torr. The typical dosing time was 60 s.

## III. RESULTS

The clean Si(100) surface consists of rows of dimers (-Si-Si-), in which each atom has one dangling bond. Saturation exposure of a clean Si(100) surface to $Cl_2$ and H atoms at appropriate conditions is known to cause all dimer dangling bonds to become terminated by those atoms while preserving the backbone dimer structure, yielding a Si(100)-$2\times1$:Cl monochloride surface and a Si(100)-$2\times1$:H monohydride surface, respectively.[25,26] The building blocks of the Si(100)-$2\times1$:H surface and the Si(100)-$2\times1$:Cl surfaces are a monohydride dimer (H-Si-Si-H) and a monochloride dimer (Cl-Si-Si-Cl), respectively, as shown in Fig. 1(a). Accordingly, the coexistence of H and Cl on the clean Si(100) surface, following either coadsorption or sequential adsorption of the two atoms, can yield mixed H-Si-Si-Cl surface species in addition to H-Si-Si-H and Cl-Si-Si-Cl.

### A. Photoemission results

Figure 2(a) displays Cl $2p$ core-level spectra (circles) of the Si(100)-$2\times1$:Cl surface and the Si(100):HCl surface that are obtained by saturating the clean Si(100) surface with $Cl_2$ and HCl at $T_s$=300 K. Chlorine has a relatively high cross section for photon stimulated desorption, which can cause systematic undercounting of the Cl coverage. However, no Cl photon stimulated desorption on the Cl/Si(100) systems was observed in consistence with several previous works that used photons from a similar bending-magnet beamline with similar photon energy.[27–29] The two Cl $2p$ spectra each has only one component, consisting of a pair of 1.60 eV spin-orbit-split peaks, and they are similar in energy and line shape but different in intensity. These observations suggest that each dissociated Cl atom from HCl reacts with a surface dangling bond, forming a Si-Cl bond and a Cl-terminated site (Cl site).[29] The intensity ratio of the two

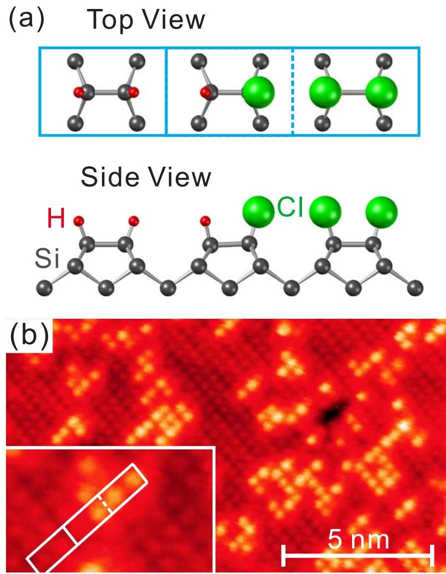


FIG. 1. (Color online) (a) Three surface species, monohydride dimer H-Si-Si-H, mixed dimer H-Si-Si-Cl, and monochloride dimer Cl-Si-Si-Cl, on Si(100) surface with mixed H and Cl termination. The smallest (red) and largest (green) spheres in the topmost layer are H and Cl atoms, respectively. (b) $15.0 \times 8.5$ nm$^2$ STM image of the mostly H-terminated Si(100)-$2\times1$ surface with 0.18 ML Cl termination (bright protrusions) measured at a sample bias $V_s$ $=2.28$ V and tunneling current $I_t=0.21$ nA. In the inset, the three neighboring rectangles enclose the three surface species described in (a). The lattice constant of a Si(100)-$1\times1$ unit cell is $a$ $=0.384$ nm.

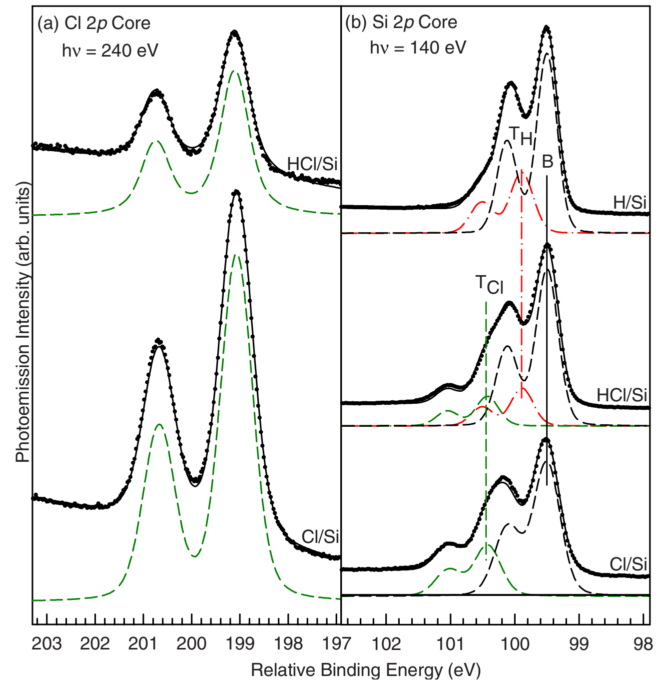


FIG. 2. (Color online) (a) Cl $2p$ and (b) Si $2p$ core-level photoemission spectra (circles) of the Si(100) surface after saturation exposure to $Cl_2$, HCl, and H atom beams at 300 K. The solid curves are fits to the spectra. The curves labeled $B$ (long dashed), $T_{Cl}$ (short dashed), and $T_H$ (dashed dot) are the results of decompositions into contributions from the bulk, Si-Cl, and Si-H species, respectively. To eliminate the band bending effect, the relative binding energy refers to the $2p_{3/2}$ line of the $B$ component (99.5 eV). Vertical lines through the $B$, $T_H$, and $T_{Cl}$ components are guides for the eyes.

Cl $2p$ spectra is $0.44\pm0.02$. The Si(100)-$2\times1$:Cl surface has nominally 1 ML of chlorine atoms (1 ML$=6.78\times10^{14}$ cm$^{-2}$). Therefore the final Cl coverage ($\Theta_{Cl}$) of the 300 K Si(100):HCl surface is approximately $0.44\pm0.02$ ML. This value is less than 0.5, which would be expected if all HCl chemisorbs dissociatively. H atoms terminate the remaining $\sim$0.56 ML dangling bonds, as the Si $2p$ spectra and STM images (to be discussed in Sec. III B) show. Accordingly, a certain percentage of HCl appears to be abstractively chemisorbed on Si(100) during the passivation process and Cl is preferentially ejected back into the vacuum.

The Si $2p$ spectra of the Si(100)-$2\times1$:Cl surface, the Si(100):HCl surface, and the Si(100)-$2\times1$:H surface are depicted in Fig. 2(b), along with their fits to constitutional components. The bottom Si $2p$ spectrum of Si(100)-$2\times1$:Cl has two components, $B$ and $T_{Cl}$, separated by about 0.92 eV. The $B$ component is responsible for emission from the bulk and the $T_{Cl}$ component is from the topmost 1 ML Si; each Si atom is terminated by Cl. Similarly, the top Si $2p$ spectrum of Si(100)-$2\times1$:H consists of two components, $B$ and $T_H$, separated by about 0.39 eV. The $T_H$ component also derives from the 1 ML outermost Si atoms that are now H terminated and, therefore, the intensity ratio $I_{T_H}/I_B$ of Si(100)-$2\times1$:H is very close to $I_{T_{Cl}}/I_B$ for Si(100)-$2\times1$:Cl. The Si $2p$ spectrum of the 300 K Si(100):HCl surface can be analyzed in terms of three components, $T_{Cl}$, $T_H$, and $B$. The intensity ratios $I_{T_H}/I_B$ and $I_{T_{Cl}}/I_B$ suggest that the coverages of surface Cl and H, $\Theta_{Cl}$ and $\Theta_H$, are about 0.45 and 0.55 ML, respectively, in close agreement with those determined from the Cl $2p$ spectra. Section IV will discuss the driving force that reduces $\Theta_{Cl}$.

### B. STM results

Upon coadsorption of both H and Cl atoms on Si(100), Cl-terminated sites (Cl-Si species or Cl sites) appear noticeably brighter than H-terminated sites (H sites) in both filled- and empty-state STM images, as shown in Figs. 1(b) and 3. In Fig. 1(b), the 0.18 ML Cl sites were produced by exposing to $Cl_2$ a mostly H-terminated Si(100) surface, in which a portion of dangling bonds were created by mild thermal annealing of the Si(100)-$2\times1$:H sample at $\sim$715 K for 50 s.[30,31] The adsorption of $Cl_2$ on an isolated dangling bond or a dangling bond pair of Si(100) has been demonstrated to be mostly abstractive and to be able to cause chain reactions;[11,30] the Si dangling bond abstracts one atom of the incident $Cl_2$ molecule, while the complementary Cl atom is scattered away from the initial abstraction site. The complementary fragment Cl atom may be captured by a second dangling bond and adsorbed there or may react with a nearby H atom to form HCl that is scattered away from the surface, leaving a new dangling bond for subsequent $Cl_2$ adsorption. The complex adsorption processes of $Cl_2$ produces large amounts of mixed Cl-Si-Si-H species even though brief ther-

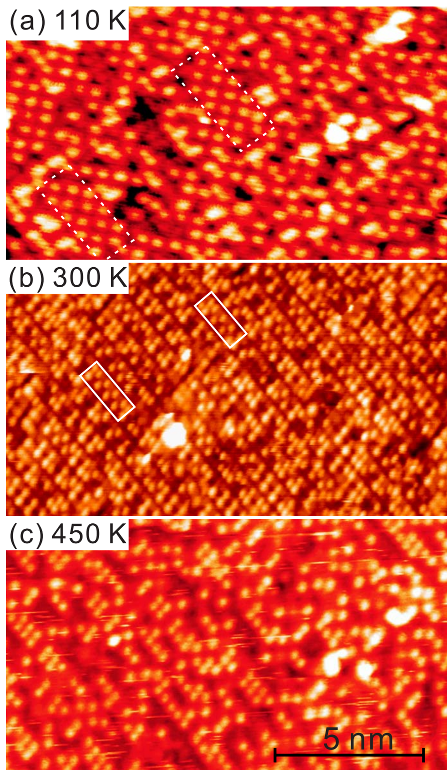


FIG. 3. (Color online) STM images of Si(100) after saturation dosage of HCl at sample temperatures of (a) 110, (b) 300, and (c) 450 K. Dashed and solid boxes enclose selected areas with a $2\times2$ and a zigzag structure, respectively. A bright protrusion corresponds to a Cl-terminated site. All images are obtained at room temperature with $I_t$=0.24 nA and $V_s$= (a) −2.46, (b) +2.27, and (c) +2.57 V. A few very bright spots on the right side of (a) and (c) and the lower middle in (b) are unknown surface species. Image size: $15\times8.5$ nm$^2$.

mal annealing yields more paired dangling bonds (-Si-Si-) than unpaired dangling bonds (-Si-Si-H).

Figure 3 shows the STM images of Si(100) after HCl has saturated the initially clean surfaces that were kept at 110, 300, and 450 K. Many bright protrusions can be discerned in the images; they are Cl sites. The H sites are not well resolved, but their termination of DBs between the Cl sites is evident and clearly revealed by the Si $2p$ spectra as discussed in Sec. III A. The coverages of Cl sites, $0.42\pm0.01$, $0.46\pm0.01$, and $0.40\pm0.01$ ML associated with adsorption at 110, 300, and 450 K, respectively, vary slightly and are in reasonable agreement with those obtained from the photoemission measurements at RT, mentioned above. In calculation of the Cl coverage, more than 2700 Cl sites were counted from a $30\times30$ nm$^2$ image. We had averaged the coverage over several images and obtained the error bar of 2% (0.01 ML). A previous study using Auger electron spectroscopy reports an even lower Cl coverage (0.25 ML at $T_s$ =100 K) and suggests that a self-site-blocking effect causes some DBs inaccessible for HCl adsorption.[24] However, no residue isolated DB is observed in Figs. 3(a)–3(c), which should appear brighter than either a H-terminated or a Cl-terminated site.[26,32]

In Fig. 3(a), many Cl sites collectively form zigzag chains and areas of well-ordered $2\times2$ structure. Since $\Theta_{Cl}/\Theta_H$ is roughly 1, a zigzag-structured chain is an ordered array of Cl-Si-Si-H mixed-hydride dimers, in which H sites and Cl sites in neighboring dimers are in antiphase with each other. The $2\times2$ structure can be regarded as a combination of more than two neighboring zigzag Cl-Si-Si-H chains with Cl sites arranged in phase. Restated, each of the Cl site in $2\times2$ areas is surrounded by four H sites, suggesting that Cl sites effectively repel each other. Figure 3(b) shows that the phase correlation of the zigzag structure both in a row and between rows is reduced upon adsorption at room temperature, yielding only short zigzag chains. At elevated substrate temperature, STM images such as Fig. 3(c) show no apparent ordering of Cl sites. More detailed analyses of the correlation between adsorption sites will be presented in Sec. IV.

## IV. DISCUSSION

### A. Mechanism for atom abstraction

As mentioned in Sec. III, both STM and photoemission data show that the DBs in the clean Si(100) surface are completely terminated by either H or Cl after HCl passivation adsorption and that the number of H-termination sites exceeds the number of Cl-terminated sites. These findings may be explained by assuming additional reaction pathways via H abstraction and Cl abstraction and that the H-abstraction pathway has a larger branching ratio than that of Cl abstraction. Notably, the relevant bond energies during HCl adsorption on the Si(100) surface are about 3.96 eV for Si-Cl, 3.30 eV for Si-H, and 4.47 eV for H-Cl.[33] Thus, the energy released during dissociative adsorption suffices to break the HCl bond ($3.96+3.30>4.47$) while those released during the H or Cl abstractions do not ($3.30, 3.96<4.47$). Therefore, unlike the $F_2$ on Si(100) and ICl on Si(111) cases,[12,13] atom abstraction here requires additional energy input during the process.

An isolated DB has its four nearest neighboring sites either H terminated or Cl terminated. When the total coverage of H and Cl sites ($\Theta=\Theta_{Cl}+\Theta_H$) is low, hardly any isolated DBs are present on the surface. The dissociative adsorption pathway, which is essentially barrierless, should predominate. As more and more DBs are terminated by H or Cl, isolated DBs emerge and increase in number with coverage as a result of random adsorption.[34] When a HCl molecule comes near and interacts with an isolated DB, a precursor state that involves the DB, the HCl molecule, and a neighboring H site (or a Cl site) may be formed.[35] Upon thermal excitation, the HCl molecule in this precursor state dissociates with one of the two fragment atoms chemisorbed and the other desorbed back into the vacuum, completing the atomically selective chemisorption. In this suggested scenario, atom abstraction is expected to occur at high coverage via a two-step process.

### B. Correlation of Cl occupancy between two adsorption sites

As described in Sec. III B, STM images show apparent local ordering of Cl sites. A correlation function for Cl sites is required to describe the partially ordered adsorbate layer.[3,36] For this aim, 20 sites that surround a centered ad-

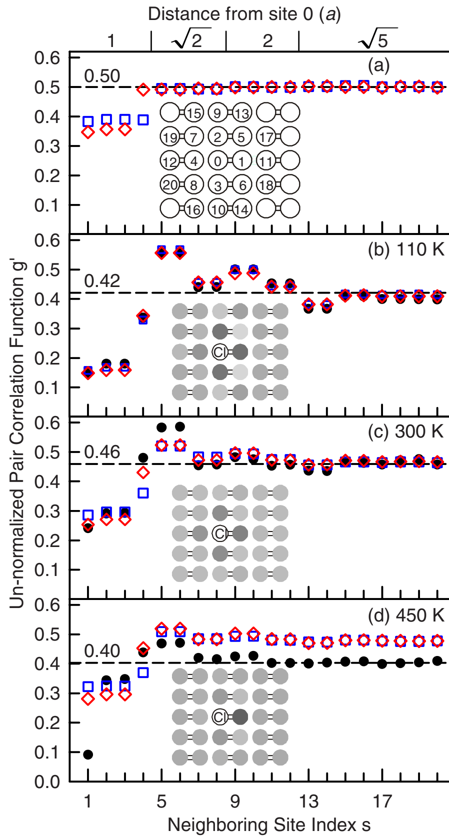


FIG. 4. (Color online) Un-normalized pair correlation function $g'$ obtained from simulation (a) program I (red diamonds) and program II (blue squares) with no fragment-adsorbate energy of interaction; (b)–(d) simulations with repulsive fragment-adsorbate energy of interaction and STM images (filled circles) of the samples in Figs. 3(a)–3(c) with $U_{intra}$=8.5 meV and $U_{inter}$=3.5 meV. The insets in (a) show the lattice of Si(100)-2×1:HCl; each circle corresponds to a H or Cl site. Numbers are site-index $s$ for sites that neighbor to the central adsorbed Cl atom ($s$=0) and distance between site $s$ and site 0 in the unit of surface lattice constant $a$. Insets of (b) and (c) are gray-scale representations of $g'$ obtained from STM images.

sorption site (labeled 0) on a Si(100) lattice with a dimerized structure are first numbered using an integer $s$, as shown in the inset of Fig. 4(a). Mirror symmetry sites, such as 2 and 3, 5 and 6, and 7 and 8, are numbered in sequence. Consider an $i$th Cl site on an STM image of the Si(100):HCl surface and label this site with the site number 0. The site occupancy $n_i(s)$ is 1.0 if site $s$ is also a Cl site; otherwise $n_i(s)$=0. The "un-normalized" pair correlation function $g'(s)$ of all Cl sites is defined as

$$g'(s) = g(s)\Theta_{\mathrm{Cl}} = \frac{1}{N_{\mathrm{Cl}}}\sum_{i=1}^{N_{\mathrm{Cl}}} n_i(s), \tag{3}$$

where $N_{\mathrm{Cl}}$ is the total number of Cl sites in that STM image and $\Theta_{\mathrm{Cl}}$ is the coverage of the Cl sites or equivalently the average Cl occupancy at any site in the image area. The use of $g'$ here, instead of the normalized pair correlation function $g$,[37] is to show in the relevant figures the Cl coverage $\Theta_{\mathrm{Cl}}$, which is also an important parameter for understanding the adsorption process.

From the definition, $g$ at a certain site $s$ can be interpreted as the ratio of two probabilities: it is the probability of finding a Cl site or the Cl occupancy at site $s$ divided by the average occupation probability $\Theta_{\mathrm{Cl}}$. The un-normalized pair correlation function $g'(s)$ measures the correlation between occupancy at the $i$th Cl site ($s$=0) and that of site $s$ around it. If $g'(s)$ is equal to $\Theta_{\mathrm{Cl}}$, then no correlation exists between site $s$ and site 0. If $g'(s)$ is larger (smaller) than $\Theta_{\mathrm{Cl}}$, then the $i$th Cl site increases (reduces) the Cl occupancy at site $s$, which is positively (negatively) correlated with site 0.

From STM images in Figs. 3(a)–3(c), the $g'$ for each $s$ can be calculated using Eq. (3); Figs. 4(b)–4(d) plot the results. To clarify the correlation between the Cl occupancies of the two neighboring sites, $g'$ for each site is also represented on a gray scale in the insets of Figs. 4(b)–4(d). As displayed in Fig. 4(b), the Cl occupancy of sites that are separated by more than two units of the lattice constant, such as $s$=15–20, has a background value of 0.42, which is the mean Cl occupancy, $\Theta_{\mathrm{Cl}}$. The occupancies for the three nearest neighboring sites, which are indexed 1–3, are markedly lower than $\Theta_{\mathrm{Cl}}$ but visibly higher for $s$=5,6,9,10, which are all two single-lattice jumps away and in the same row as site 0.

Figure 4(c) plots results concerning room-temperature adsorption. They reveal essentially the same trends: the $g'$ values at sites within two units of the lattice constant ($s$=1–12) deviate from the mean occupancy but with a lower variation than those in Fig. 4(b). For the 450 K Si(100):HCl surface, the variations of $g'$ are even smaller except at $s$=1. Since the two sites $s$=0 and 1 are located on the two sides of a dimer, the small $g'(1)$ indicates that the probability of finding two Cl sites on the same dimer is significantly lower than $\Theta_{\mathrm{Cl}}$. In view of the fact that Cl and H sites are mobile at elevated temperature,[38,39] the negative correlation between Cl occupancy of the two sites (0 and 1) suggests that Cl-Si-Si-H is thermodynamically favored over the monochloride and monohydride dimers.

Since Cl sites on the 110 K Si(100)-2×1:HCl surface have a higher degree of ordering than those obtained at higher $T_s$, the following discussion focuses on the 110 K adsorption. In the inset of Fig. 4(b), the sites farther from a central Cl site are moderately gray, corresponding to average occupancy. Sites 1–3 are darker, indicating their statistically lower Cl occupancy probability and therefore higher H occupancy. The substantially higher probability of H termination at sites 1–3 suggests the following two possible occurrences. (1) When the dangling bond at site 0 collects the Cl atom from HCl, the complimentary H atom prefers the nearest neighboring site in the same row. (2) Dissociated Cl atoms dissociated upon subsequent impingements of HCl on these three nearest neighboring sites, 1–3, are driven away. The occupancy of the other immediate neighbor, i.e., site 4, is only slightly lower than the average, suggesting that the site correlation is weaker in the neighboring row than that in its row. The second nearest neighbors in the same row, sites 5 and 6, have moderately higher occupancy; this result is consistent with the formation of short zigzag chains.

### C. Monte Carlo simulations

As discussed in Sec. IV A, both dissociative and abstractive pathways occur during the saturation of Si(100) by HCl. The saturation process consists of a sequence of chemisorption of individual HCl molecules. Studies showed that separate adatoms in dissociative adsorption of many diatomic molecules on the clean Si(100) surface are usually one or two atom units away from each other.[26,30,40] Accordingly, we first model HCl chemisorption as a process in which, upon striking on one dangling bond, one of the two separated atoms (referred to as the first atom $A$) is trapped and chemisorbed on the dangling bond and the second atom (referred to as $B$) is chemisorbed on one of the nearest or second nearest active sites (dissociative adsorption) or desorbs from the surface (atom abstraction).

To understand the pair correlation functions extracted from the STM images, Monte Carlo simulations were performed on a square area of $300 \times 300$ unit cells that are organized into $150 \times 300$ dimers. Initially, all the $9 \times 10^4$ sites are set active for H or Cl termination; they are DBs. The simulation program models the irreversible adsorption or random sequential adsorption of HCl from $\Theta = 0$ to 1.0 ML. Two steps are involved for each simulated adsorption process of a HCl molecule: the first step is to place atom $A$ and the second step, atom $B$. In the first step, an active site is randomly selected and atom $A$ is chemisorbed on the spot (site 0). Cl and H are assumed to have an equal probability to be atom $A$; the probability for Cl to be atom $A$, $P_{\mathrm{Cl}}$, is thus 0.5.

The second step in the simulation involves three cases. Case 1: at least one of three nearest neighboring vacant sites on the same dimer row ($s=1-3$) is still active. Then atom $B$ lands with equal probability at one of those active sites, i.e., $P_{B,nn}=1/N_a$, where $P_{B,nn}$ is the probability for atom $B$ to land on one nearest neighboring active site and $N_a$ is number of active sites among $s=1-3$. The reason to choose only among $s=1-3$ is that the correlation of occupancy between sites in the same row is markedly stronger than that in adjacent row, as discussed in Sec. IV B. The simulation based on this assumption is referred to as program I. However, site 4 might be arguably equivalent to sites 1–3. For comparison, program II thus randomly selects one active site among sites 1–4, i.e., $P_{B,nn}=1/N_a$, with $N_a=1-4$. Case 2: the immediate neighboring sites are all occupied. Then program I (II) randomly selects one active site among the second nearest neighbors $s=4-8$ (5–8) with equal probability $P_{B,snn}=1/N_a$ with $N_a=1-5$ (1–4). Case 3: all eight neighboring sites 1–8 are occupied. In this case, both programs I and II assume that atom $B$ is ejected back to vacuum and, therefore, an $A$ abstraction occurs. Based on the above-mentioned minimum set of rules, programs I and II generate the arrangement of H and Cl sites from $\Theta=0$ to 1.0 ML; a selected area at $\Theta = 1.0$ by program I is shown in Fig. 5(a). No obvious ordered areas can be found in Fig. 5(a), in disagreement with the ordering found in STM images. The branching ratios for the H abstraction, the Cl abstraction, and the dissociative adsorption as a function of $\Theta$ during the simulation are displayed in Fig. 6(a). According to Fig. 6(a), atom abstractions take place when $\Theta$ exceeds ~0.5 ML and becomes increasingly significant only when $\Theta$ approaches 1.0; H abstraction and Cl abstraction have essentially the same occurrence probabilities because the programs treat H and Cl equally.

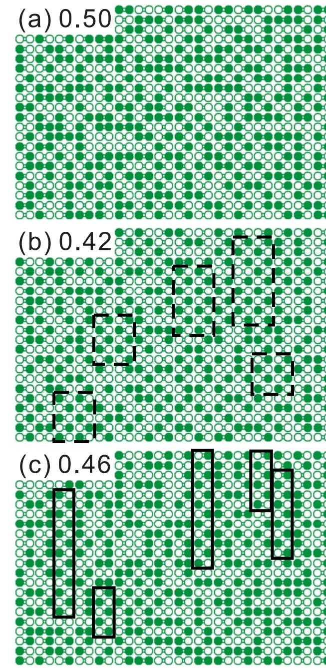


FIG. 5. (Color online) Simulated distributions of coadsorbed H (circles) and Cl (filled circles) sites on Si(100)-$2 \times 1$ at (a) and (b) 110 and (c) 300 K. Coverages of Cl-terminated sites in monolayer are given. Dashed and solid boxes enclose selected areas with a $2 \times 2$ and a zigzag structure, respectively. In (a) fragment-adsorbate energies of interaction are 0. In (b) and (c), the repulsive energies are $U_{intra}=8.5$ meV and $U_{inter}=3.5$ meV.

The corresponding $g's$ can be calculated from the simulated arrangement [Fig. 5(a)]; a set of typical results is dis-

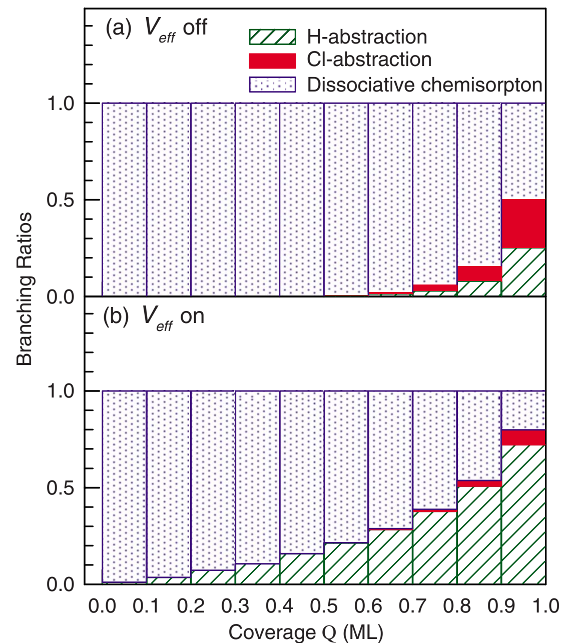


FIG. 6. (Color online) Branching ratios of three adsorption pathways as a function of $\Theta$ using program I with the effective substrate interaction $U_{eff}$ (a) off and (b) on. $R_{\mathrm{Cl}}$ used is 0.5.

played in Fig. 4(a). Figure 4(a) shows that $\Theta_{Cl}$ is 0.5 even though a fraction of adsorption takes place via the abstractive reaction pathways. This is because H abstraction and Cl abstraction have the same occurrence probabilities. Program I (II) results in lower values of $g'$ for $s=1-3$ (1–4) because the complementary fragment $B$ atom (H) initially seeks dangling bonds that are immediate neighbors to $A$ (Cl) and, therefore, reduces the probability of Cl occupation. The occupancy of all other sites is approximately 0.5, indicating no correlation between sites 0 and $s$. These results strongly disagree with the experimental data and additional interactions during the saturation adsorption should be considered.

### D. Simulation with the introduction of fragment-adsorbate interactions

Once chemisorbed, H and Cl atoms are immobile at RT or below on the silicon substrates because of large diffusion barriers.[39,40] Thus, the correlation between Cl adsorption sites is established during the adsorption process and before the formation of Cl-Si bonds. Hence, the partial ordering of Cl sites suggests that forces between a Cl atom (Cl fragment) and its surrounding adsorbates are already present before the chemisorption of a Cl fragment is completed. Assumed to be short ranged, the forces between a fragmented Cl atom, either atom $A$ or atom $B$, at a DB site ($s=0$) and a Cl site at $s=1-4$ can be described by effective interactions, $U_{01}$, $U_{02}$, $U_{03}$, and $U_{04}$, respectively. The fragment-adsorbate interactions between Cl and H and between H and H are assumed to be negligible.[8] The effective substrate interaction $U_{eff}$ experienced by the Cl fragment is the sum of the four energies $U_{0s}$ ($s=1-4$). In Figs. 4(b) and 4(c), the $g's$ for $s=1-3$, which sites are located in the same dimer row, are similar. Therefore the simulation programs equalize the interaction energy $U_{intra}=U_{01}=U_{02}=U_{03}$ for simplicity, where $U_{intra}$ denotes intrarow interaction.

With the introduction of the effective nearest neighboring Cl-fragment–Cl-adsorbate interaction, programs I and II are modified accordingly. In the first step, the probabilities for atom $A$ to be Cl are reduced by a Boltzmann factor according to

$$P_{Cl}=R_{Cl}e^{-(U_{eff}/kT)}=R_{Cl}e^{-[(U_{01}+U_{02}+U_{03}+U_{04})/kT]}, \quad (4)$$

where $R_{Cl}$ indicates the initial probability of Cl adsorption on a DB and is 0.5, assuming no atomic chemical selectivity in the gas-surface interaction.[12] The probability for atom $A$ to be H, $P_H$, is $1-P_{Cl}$. In the second step, no change in programs I and II is made if the atom $B$ is H. If atom $B$ is Cl, then program I randomly selects one active site among the first nearest neighbors $s=1-3$ ($s=4-8$) for case 1 (case 2) with unequal probabilities according to

$$P_{Cl,s}=\frac{1}{Z}e^{-(U_{eff,s}/kT)}, \quad (5)$$

where $U_{eff,s}$ is the effective interaction energy seeing from site $s$ and $Z$ is the normalization factor, i.e.,

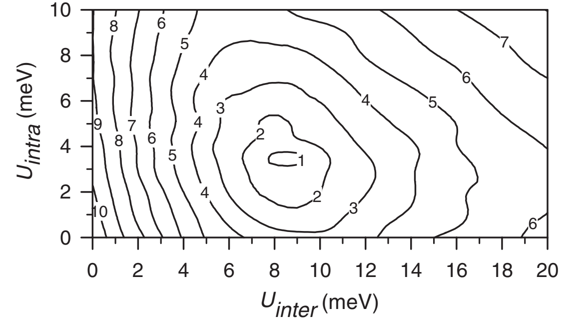


FIG. 7. Contour plot of standard deviation $\sigma(100)$ between the simulation and STM result (110 K) as functions of repulsive interacting energies $U_{intra}$ and $U_{inter}$. Simulated results more closely match STM measurements in areas where $\sigma$ is smaller.

$$Z=\sum_{j=1}^{N_a} e^{-(U_{eff,j}/kT)}. \quad (6)$$

When site $s$ is selected, the programs also reduce the probability for atom $B$ (Cl) to be chemisorbed by the same Boltzmann factor $e^{-(U_{eff,s}/kT)}$. This assumption effectively breaks the evenly balanced H-abstraction and Cl-abstraction occurrence ratios and is needed in order to match the experimentally measured temperature dependent $\Theta_{Cl}$. Again, all simulations of HCl passivation processes were conducted on an area with $300\times150$ dimers. The $g's$ for site $s$ obtained from the computer simulations, $g'_{sim,s}$, is compared with that from the STM measurement, $g'_{exp,s}$, in terms of the standard deviation $\sigma$, which is defined as

$$\sigma=\sqrt{\frac{1}{n}\sum_{s=1}^{n}(g'_{sim,s}-\overline{g'_{exp,s}})^2}, \quad (7)$$

where $n=20$ is the total number of calculated sites. A smaller $\sigma$ indicates a better match between the simulation result and the corresponding experimental measurement. Figure 7 shows a contour plot of standard deviation $\sigma$ using program I for 110 K adsorption as functions of the repulsion energies $U_{intra}$ and $U_{inter}=U_{04}$, where $U_{inter}$ denotes inter-row interaction. As Fig. 7 indicates, the repulsion energies of about $U_{intra}=8.5\pm2.0$ meV and $U_{inter}=3.5\pm2.0$ meV give the best fit. This corresponds to $U_{eff}\approx29$ meV at most if all neighboring sites are occupied. The intrarow energy of fragment-adsorption interaction is significantly lower than the repulsion energy (61 meV) between two adjacent adsorbate-adsorbate dimers ($4\times8.5<61$),[8] perhaps because a Cl fragment is a neutral radical while a Cl adsorbate is negatively charged. Using these energies, the distributions of Cl and H sites are simulated for adsorption at 110, 300, and 450 K (not shown) and displayed in Figs. 5(b) and 5(c), respectively. Figures 4(a)–4(c) plot the corresponding $g's$ and the branching ratios for the three adsorption reactions are shown in Fig. 6(b). As Figs. 4(b) and 4(c) show, program I gives a slightly better overall fit, while both programs I and II reproduce well the overall trends in the $g's$. With the introduction of the effective interaction, Fig. 6(b) shows that

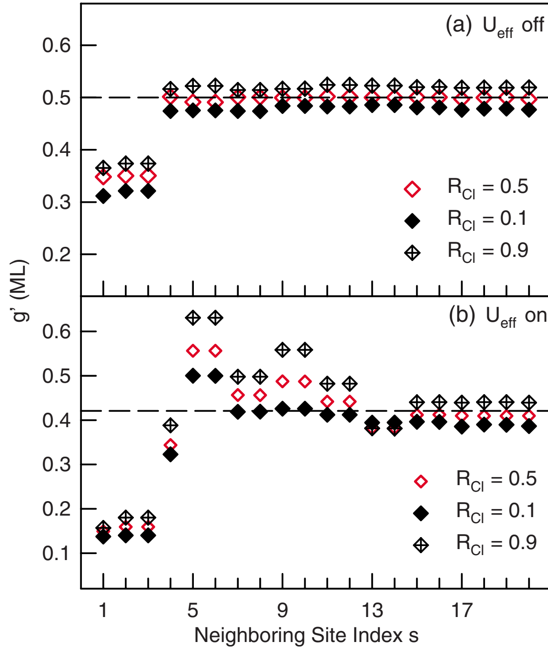


FIG. 8. (Color online) Un-normalized pair correlation function $g'$ obtained by program I with three $R_{\mathrm{Cl}}$ values as labeled. The repulsive fragment-adsorbate energies used are (a) $U_{intra}=U_{inter}=0$ and (b) $U_{intra}=8.5$ meV and $U_{inter}=3.5$ meV.

atom abstractions occur at low $\Theta$ and at substantially higher rates.

Despite the successful reproduction of $g's$ at low substrate temperature, the simulation results for adsorption at elevated temperature do not agree with the experimental ones, as shown in Fig. 4(d). In view of the $U_{eff}\approx 29$ meV, which is approximately $kT$ at room temperature, this is not surprising.

Equation (4) reveals that the effective substrate interaction energy $U_{eff}$ can reduce the probability $P_{\mathrm{Cl}}$ that a fragment Cl atom bonds with a DB that has at least one nearest neighboring Cl site. However, a reduced value of $R_{\mathrm{Cl}}$ can lower $P_{\mathrm{Cl}}$ as well. As mentioned above, the simulation programs assume that H or Cl is adsorbed with equal probability on a DB that is randomly struck by a HCl molecule such that $R_{\mathrm{Cl}}=0.5$. Simulations by program I using various $R_{\mathrm{Cl}}$ and $U_{eff}=0$ give rather featureless $g's$ for $s>4$, as shown in Fig. 8(a), and, therefore, fail to predict the measurements accurately. $\Theta_{\mathrm{Cl}}$ also rises (falls off) with increasing (decreasing) $R_{\mathrm{Cl}}$; this is expected since the Cl abstraction is enhanced by a larger $R_{\mathrm{Cl}}$. Giving the set of the repulsion energies found above, program I reproduces again the main features of the unnormalized pair correlation function $g'$ over a large range of $R_{\mathrm{Cl}}$. These findings further enlighten the presence of the repulsive forces between fragment atoms and adsorbates as well as the repulsion energies found above.

## V. CONCLUSIONS

Upon collision with a surface, a diatomic molecule may bounce back or may be molecularly adsorbed or cleaved into two fragments. If the molecule is cleaved, the two fragments interact readily with the surface as well as the adsorbates in the vicinity of the reaction site before being adsorbed or reflected back into vacuum. Quantitative measurement of the fragment-adsorbate interaction is not an easy task considering its transient and many-body effects. To this end, this work investigates the adsorption kinetics of a simple diatomic molecule, i.e., HCl, on the Si(100)-2×1 surface by integrating a spectroscopic measurement of core-level photoemission, atomic resolved STM imaging, and Monte Carlo simulations. Experimental results reveal that saturation exposure to HCl at a sample temperature between 110 and 450 K causes all dangling bonds on the clean Si(100) surface to be terminated by the two fragments, H and Cl atoms. The HCl-saturated Si(100) surface exhibits the following characteristics:

(1) the number of H-terminated sites exceeds that of Cl-terminated ones by more than 10%;

(2) at a substrate temperature of 110 K, the mixed Cl-terminated and H-terminated sites exhibit short-range order and form 2×2 patches; and

(3) the degree of the mixed-adsorbate ordering is reduced as the substrate temperature increases.

To reproduce well the experimental results, we have performed Monte Carlo simulations and demonstrated the following findings:

(1) The adsorption of HCl proceeds by the combination of a dissociative mechanism and atom abstraction in favor of H fragments over Cl.

(2) During dissociative chemisorption on surfaces, the fragment-adsorbate interactions are present and cause the partial order of the adsorbates.

(3) Reliable values of the fragment-adsorbate interaction energies can be extracted by comparing the simulated and measured occupancy pair correlation functions. If a Cl fragment is in the same dimer row as another Cl adsorbate, then the energy of their interaction energy $8.5\pm 2.0$ meV exceeds that and $3.5\pm 2.0$ meV when they are in adjacent rows.

## ACKNOWLEDGMENTS

The authors wish to acknowledge the financial support of the National Science Council of Taiwan (Contract No. NSC 95-2112-M007-067-MY4 for D.-S.L.) and the Sandwich Program sponsored by the German Academic Exchange Service (DAAD).

*Author to whom correspondence should be addressed; dslin@phys.nthu.edu.tw

[1] T. J. Rockey, M. Yang, and H.-L. Dai, J. Phys. Chem. B **110**, 19973 (2006).
[2] I. Brihuega, A. Cano, M. M. Ugeda, J. J. Saenz, A. P. Levanyuk, and J. M. Gomez-Rodriguez, Phys. Rev. Lett. **98**, 156102 (2007).
[3] L. Österlund, M. Ø. Pedersen, I. Stensgaard, E. Laegsgaard, and F. Besenbacher, Phys. Rev. Lett. **83**, 4812 (1999).
[4] A. Bogicevic, S. Ovesson, P. Hyldgaard, B. I. Lundqvist, H. Brune, and D. R. Jennison, Phys. Rev. Lett. **85**, 1910 (2000).
[5] P. Hyldgaard and M. Persson, J. Phys.: Condens. Matter **12**, L13 (2000).
[6] G. A. Somorjai, *Introduction to Surface Chemistry and Catalysis* (Wiley, New York, 1994).
[7] V. P. Zhdanov, Langmuir **17**, 1793 (2001).
[8] D. Chen and J. J. Boland, Phys. Rev. Lett. **92**, 096103 (2004).
[9] H. Xu and I. Harrison, J. Phys. Chem. B **103**, 11233 (1999).
[10] B. G. Briner, M. Doering, H.-P. Rust, and A. M. Bradshaw, Science **278**, 257 (1997).
[11] I. R. McNab and J. C. Polanyi, Chem. Rev. (Washington, D.C.) **106**, 4321 (2006).
[12] Y. Liu, D. P. Masson, and A. C. Kummel, Science **276**, 1681 (1997).
[13] Y. L. Li, D. P. Pullman, J. J. Yang, A. A. Tsekouras, D. B. Gosalvez, K. B. Laughlin, Z. Zhang, M. T. Schulberg, D. J. Gladstone, M. McGonigal, and S. T. Ceyer, Phys. Rev. Lett. **74**, 2603 (1995).
[14] M. Binetti, O. Weisse, E. Hasselbrink, A. J. Komrowski, and A. C. Kummel, Faraday Discuss. **117**, 313 (2000).
[15] M. Binetti and E. Hasselbrink, J. Phys. Chem. B **108**, 14677 (2004).
[16] M. R. Tate, D. Gosalvez-Blanco, D. P. Pullman, A. A. Tsekouras, Y. L. Li, J. J. Yang, K. B. Laughlin, S. C. Eckman, M. F. Bertino, and S. T. Ceyer, J. Chem. Phys. **111**, 3679 (1999).
[17] A. J. Komrowski, J. Z. Sexton, A. C. Kummel, M. Binetti, O. Weiße, and E. Hasselbrink, Phys. Rev. Lett. **87**, 246103 (2001).
[18] J. G. E. Gardeniers and L. J. Giling, J. Cryst. Growth **115**, 542 (1991).
[19] J. M. Hartmann, V. Loup, G. Rolland, and M. N. Semeria, J. Vac. Sci. Technol. B **21**, 2524 (2003).
[20] H. Habuka, T. Suzuki, S. Yamamoto, A. Nakamura, T. Takeuchi, and M. Aihara, Thin Solid Films **489**, 104 (2005).
[21] A. Sánchez-Castillo, G. H. Cocoletzi, and N. Takeuchi, Surf. Sci. **521**, 95 (2002).
[22] M. P. D'Evelyn, Y. L. Yang, and S. M. Cohen, J. Chem. Phys. **101**, 2463 (1994).
[23] B. I. Craig and P. V. Smith, Surf. Sci. **262**, 235 (1992).
[24] Q. Gao, C. C. Cheng, P. J. Chen, W. J. Choyke, and J. T. Yates, Jr., Thin Solid Films **225**, 140 (1993).
[25] J. J. Boland, Adv. Phys. **42**, 129 (1993).
[26] I. Lyubinetsky, Z. Dohnálek, W. J. Choyke, and J. T. Yates, Phys. Rev. B **58**, 7950 (1998).
[27] T.-W. Pi, S.-F. Tsai, C.-P. Ouyang, J.-F. Wen, and R.-T. Wu, Surf. Sci. **488**, 387 (2001).
[28] L. S. O. Johansson, R. I. G. Uhrberg, R. Lindsay, P. L. Wincott, and G. Thornton, Phys. Rev. B **42**, 9534 (1990).
[29] D. S. Lin, J. L. Wu, S. Y. Pan, and T. C. Chiang, Phys. Rev. Lett. **90**, 046102 (2003).
[30] S.-S. Ferng, S.-T. Wu, D.-S. Lin, and T. C. Chiang, J. Chem. Phys. **130**, 164706 (2009).
[31] M. McEllistrem, M. Allgeier, and J. J. Boland, Science **279**, 545 (1998).
[32] J. J. Boland, Science **262**, 1703 (1993).
[33] M.-F. Hsieh, D.-S. Lin, and S.-F. Tsay, Phys. Rev. B **80**, 045304 (2009).
[34] R. S. Nord and J. W. Evans, J. Chem. Phys. **82**, 2795 (1985).
[35] Y. A. Mantz, F. M. Geiger, L. T. Molina, M. J. Molina, and B. L. Trout, Chem. Phys. Lett. **348**, 285 (2001).
[36] G. Wiatrowski, J. C. Le Bosse, J. Lopez, and I. Zasada, Surf. Sci. **265**, 229 (1992).
[37] J. Trost, T. Zambelli, J. Wintterlin, and G. Ertl, Phys. Rev. B **54**, 17850 (1996).
[38] G. A. de Wijs and A. Selloni, Phys. Rev. Lett. **77**, 881 (1996).
[39] J. H. G. Owen, D. R. Bowler, C. M. Goringe, K. Miki, and G. A. D. Briggs, Phys. Rev. B **54**, 14153 (1996).
[40] G. J. Xu, A. W. Signor, A. Agrawal, K. S. Nakayama, B. R. Trenhaile, and J. H. Weaver, Surf. Sci. **577**, 77 (2005).